Is Dissociation of HCl in DMSO Clusters Bistable?

Debopriya Sadhukhan,[1] Po-Jen Hsu,[2] Jer-Lai Kuo,*[2] and G. Naresh Patwari*[3]

[1] IITB-Monash Research Academy, Indian Institute of Technology Bombay, Mumbai 400076, India

[2] Institute of Atomic and Molecular Sciences, Academia Sinica, Taipei 10617, Taiwan.

E-mail: jlkuo@pub.iams.sinica.edu.tw

[3] Department of Chemistry, Indian Institute of Technology Bombay, Mumbai 400076 India. E-mail: naresh@chem.iitb.ac.in

ABSTRACT

The dissociation of HCl embedded in DMSO clusters was investigated by projecting the solvent electric field along the HCl bond using B3LYP-D3/6-31+G(d) and MP2/6-31+G(d,p) levels of theory. A large number of distinct structures (about 1500) consisting of up to five DMSO molecules were considered in the present work for statistical reliability. The B3LYP-D3 calculations reveal that the dissociation of HCl embedded in DMSO clusters requires a critical electric field of 138 MV cm^{-1} along the H–Cl bond. However, a large number of exceptions wherein the electric field values much higher than the critical electric field of 137 MV cm^{-1} did not result in dissociation of HCl in addition to several cases wherein the HCl dissociates with an electric field less than the critical electric field. On the other hand, the MP2 level calculations reveal that the critical electric field for the HCl dissociation is about 181 MV cm^{-1} with almost no exceptions. The B3LYP-D3 calculations suggest that the dissociation of HCl embedded in DMSO clusters is bistable, which is an artefact, suggesting care must be exercised in interpreting processes proton transfer. The answer to the question raised as the title of this paper is NO.

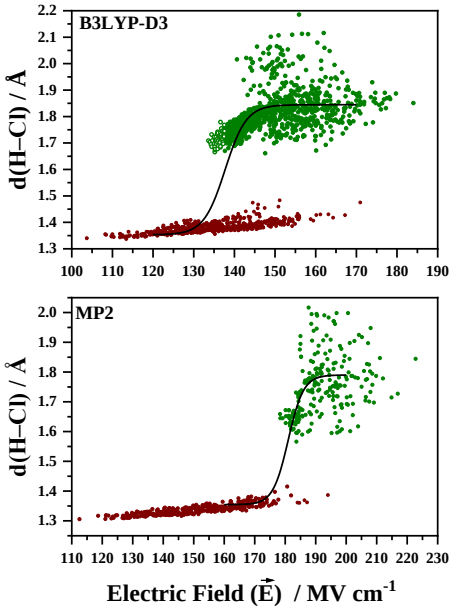

INTRODUCTION

Mineral acids are one of the most commonly used chemicals in industries.[1] From the synthesis of other chemicals to manufacturing pesticides, PVC pipes, etc., these mineral acids are used everywhere. Because of their widespread use, their importance in industry and research cannot be overstated. In general, an acid is considered to be a strong acid if it dissociates completely in an aqueous solution, and the strength of an acid is determined by its pK_a value, which is a negative logarithm of the acid dissociation constant, K_a. However, this pK_a value depends on the solvent used, for instance, pK_a of HCl in water and DMSO are -7.0 and 1.8, respectively,[2,3] which also suggests that the acid dissociation mechanism could be solvent dependent. On the other hand, DMSO is a widely used solvent due to its amphipathic nature,[4–7] with applications ranging from medicinal chemistry, wherein it is used as a drug-delivery vehicle,[8] and cell cryopreservation, and several others.[9] It has been reported that in the neat liquid form DMSO molecules self-associate to form polymer chains through the interactions between its sulfur and oxygen atoms.[4,8] However, these formed self-associated DMSO molecules are not stable, but it gets dissociated due to the presence of proton-donor solvents, and the effect of elevated temperatures. Binary mixtures of DMSO and other co-solvents are also known to be heterogeneous.[10–13] In the case of DMSO-water mixture, the maximum deviation from the ideal mixing behavior occurs around 33% mole fraction of DMSO.[10] The existence of different types of aggregates in the DMSO-water mixture is believed to be the reason behind this heterogeneity. A similar type of behavior has also been observed in DMSO-glycerol[9] and DMSO-methanol mixtures.[10]

In this work, an effort has been made to understand the HCl dissociation mechanism in DMSO at a molecular level. When an acid is dissociated, the resulting ion pair gets stabilized by the solvent molecules present in the system. Therefore, the dissociation of an acid in a particular solvent doesn't only depend on the ability of the acid to transfer a proton to the surrounding solvent molecules but also depends on the ability of the solvent to accept the proton from the acid molecule. It has been reported that acid will get dissociated in a particular solvent if the stability of the dissociated acid-solvent cluster is greater than the stability of the undissociated acid-solvent cluster.[11–16] However, it was shown that the acid dissociation mechanism of HCl in water and reported that the stabilization energy of the HCl-water cluster is not the only criteria for the acid

to be dissociated in water, and the orientation of the water molecules around the HCl molecule also plays a pivotal role in the acid dissociation process.[14] It was also reported that in some HCl-water clusters the HCl remains undissociated, even though in those structures the number of water molecules and their stabilization energy were almost identical to the dissociated HCl-water clusters. Therefore, to investigate the acid-dissociation mechanism at a molecular level, getting accurate geometries is of utmost importance. In the present work, the role of cluster geometry for the HCl embedded in DMSO molecules and the consequent dissociation of acid (the proton transfer process) is explored using long-range dispersion corrected DFT along with MP2 level calculations.

METHODOLOGY

The structures of HCl-$(DMSO)_n$ [*n*=2-5] clusters were obtained by a combination of structural random search and screening techniques. To begin with, a cubic cell of the size 4x4x4 (in angstrom) was defined, and *n*+1 points were randomly distributed in the cell. These points will serve as the center of mass (COM) of the molecules. To avoid the unphysical configurations, a minimum distance constraint of 5 Å was imposed between the points in the cell. Following, *n*+1 molecules (*n* for DMSO and 1 for HCl) were placed on these points with arbitrary orientation. By repeating these steps, thousands of random configurations for the HCl-$(DMSO)_n$ [*n*=2-5] clusters were obtained. To reduce the computational cost of the DFT optimization, these structures were pre-optimized using DFTB3 semi-empirical method[15–18] using CP2K software.[19] Following, the duplicated configurations were removed using the shape similarity screening technique[20] with a high similarity index threshold of 0.99. Distinct structures were re-optimized by B3LYP/6-31+G(d) with GD3 long-range dispersion correction (B3LYP-D3).[21] After the geometric optimization, the screening process using shape similarity was carried out to once again remove the duplicated structures, if any. Finally, several representative HCl-$(DMSO)_{2-5}$ clusters from the B3LYP-D3 data were re-optimization at the MP2/6-31+G(d,p) level of theory. All the structure optimizations were carried out using Gaussian software suite.[22] The normal mode analysis are performed to ensure that the true local minima were found. This multi-stage optimization scheme efficiently obtains a set of well-converged structures at a higher level of theory and has been successfully applied to hydrogen-bonded[23,24] and π–stacked complexes. [25,26]

To understand the dissociation of HCl embedded in DMSO solvent clusters, the electric field calculations were carried.[14,27-30] These calculations elucidate the effect of charge distribution around an HCl molecule as a consequence of a change in the arrangement of the surrounding solvent molecules. The electric field along the H–Cl bond was calculated by replacing the H and the Cl atoms with ghost atoms and retaining the rest of the DMSO cluster. Following, the molecular electrostatic potential (MESP) arising from all the DMSO molecules at the position of H and Cl was calculated using the equation

$$V_{H/Cl} = \sum_{A \neq H,\mathrm{Cl}} \frac{Z_A}{|\vec{R}_A - \vec{R}_{H/Cl}|} - \int \frac{\rho(\vec{r}) d^3\vec{r}}{|\vec{r} - \vec{R}_{H/Cl}|} \qquad (1)$$

Where Z_A is the nuclear charge of atom A located at $\vec{R}_A$ while $\vec{R}_H$ and $\vec{R}_{Cl}$ are the positions of H and Cl atoms, and $\rho(\vec{r})$ is the electron density of the molecule and $\vec{r}$ is a dummy integration variable. The projection of the electric field $\vec{E}$ onto the H–Cl bond was calculated as the gradient of the electrostatic potential along the bond axis

$$\vec{E} = -\nabla V = \frac{-(V_{Cl} - V_H)}{|(\vec{R}_{Cl} - \vec{R}_H)|} \qquad (2)$$

In equation (2), V_H and V_{Cl} are the measure of the electrostatic potential at the position of H and Cl atoms due to all the electrons and the nuclei that make up the DMSO cluster around the HCl molecule. The optimization of the structures and the MESP calculations for the estimation of electric fields were carried out using the Gaussian-6 suite of programs.[22]

RESULTS and DISCUSSION

The structures of the HCl-$(DMSO)_n$ [n=2-5] were obtained by structure search algorithm followed by optimization using B3LYP-D3/6-311+G(d,p) level of theory, which resulted in a total of 1477 structures with 21, 166, 441, and 849 clusters with two, three, four and five DMSO molecules, respectively, in which the calculated electric field along the H–Cl bond is more than −100 MV cm^{-1} and are considered. The negative electric field along the H–Cl bond, which indicates the stabilization due to hydrogen bonding.[30] Figure 1A shows the plot of H–Cl distance against the electric field along the H–Cl bond, which clearly shows two sets of data corresponding to 509 undissociated (H–Cl distance < 1.49 Å) and

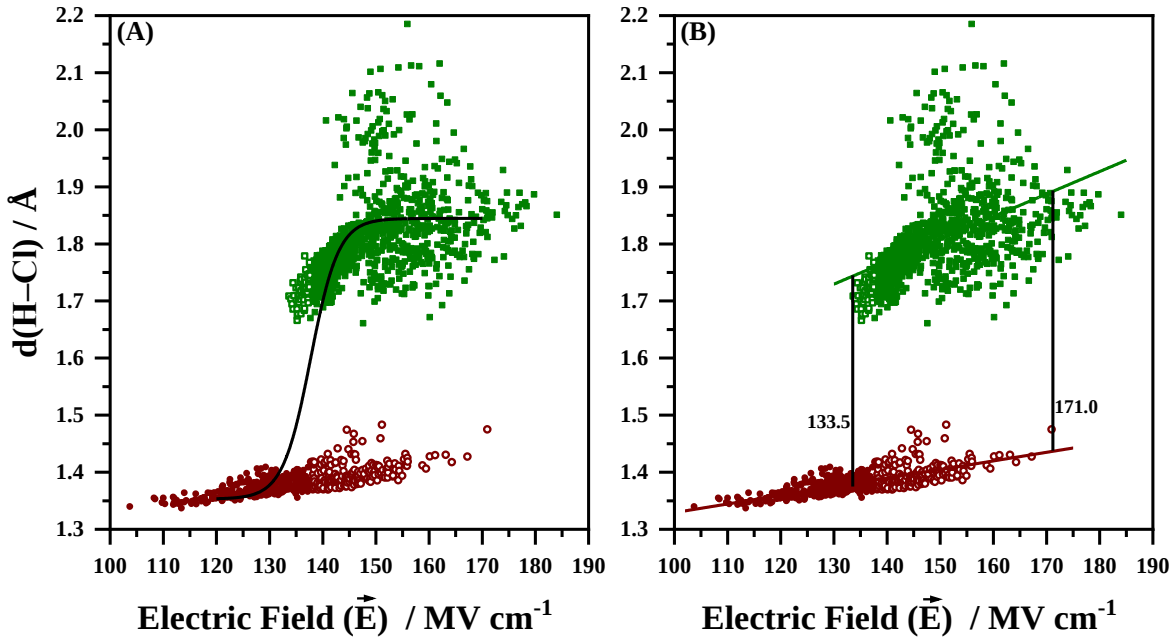

Figure 1. The plot of H–Cl distance against electric field calculated along the H–Cl bond in HCl(DMSO)$_n$ [n=2-5] clusters at B3LYP-D3/6-311+G(d,p) level of theory. The data points in red circles and green squares correspond to the undissociated and dissociated HCl molecule, respectively. In (A) the solid curve is a non-linear Boltzmann sigmoidal fit to the data points shown in red closed circles and green closed squares with an R^2 value of 0.789 with the point of inflection at 137.7 MV cm^{-1}. The data points shown as red open circles and green open squares have been omitted from the fitting. In (B) the red and green lines are the linear least-square fits to the data points corresponding to undissociated and dissociated HCl molecule. In both (A) and (B) the solid circles and solid squares correspond to normal data points, while the open circles and open squares are exceptions to the sigmoidal fitting. In (B) the region between 133.5 and 171 MV cm^{-1} is bistable.

968 dissociated HCl (H–Cl distance > 1.66 Å) molecules embedded in DMSO clusters. Boltzmann sigmoidal fit to the data points yields a poor-fitting with an R^2 value of 0.789 with the point of inflection corresponding to 137.7 MV cm^{-1}. However, unlike the dissociation of HCl in water clusters which yields a critical electric field of 193 MV cm^{-1},[14] the critical electric field in the present case is not a good measure of the HCl dissociation process in DMSO clusters. Based on the sigmoidal fitting, the entire data set consisting of HCl-(DMSO)$_n$ clusters is classified into four categories: (a) structures with undissociated HCl and the electric field lower than the critical electric field (320 data points; red closed circles in Figure 1), (b) structures with undissociated HCl with the electric field higher than the critical electric field (189 data points, red open circles in Figure 1), (c) structures

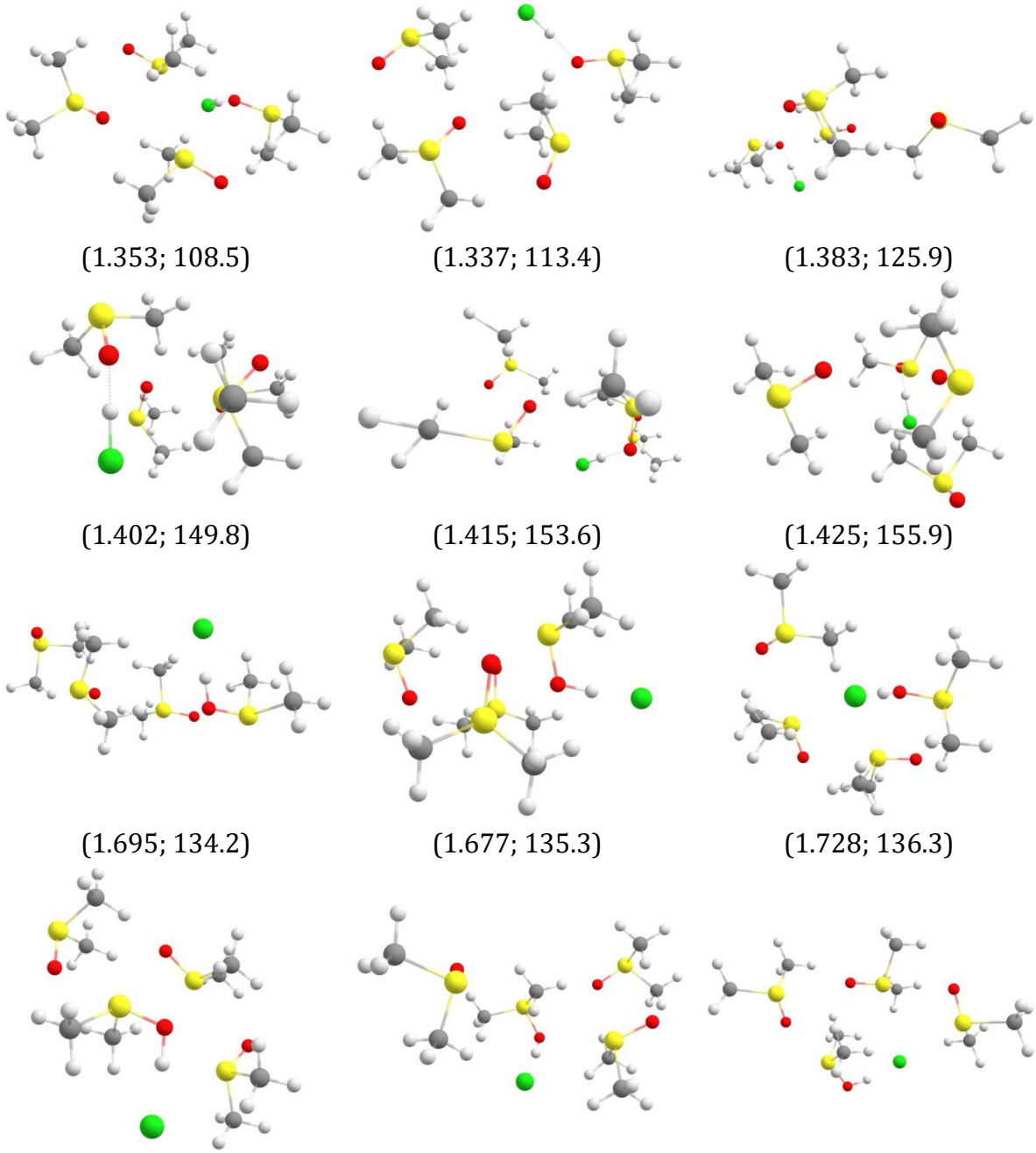

Figure 2. Representative structures for the four categories of HCl-$(DMSO)_4$ clusters. First row: Structures with undissociated HCl and electric field lesser than the critical electric field. Second row: Structures with undissociated HCl and electric field greater than the critical electric field. Third row: Structures with dissociated HCl and electric field lesser than the critical electric field. Fourth row: Structures with dissociated HCl and electric field greater than the critical electric field. Against each structure the corresponding H–Cl distance (in Å) and the electric field along the H–Cl bond (in MV cm^{-1}) are given in parenthesis.

with dissociated HCl and electric field lower than the critical electric field (50 data points, green open circles in Figure 1), and (d) structures with dissociated HCl and the electric field is higher than the critical electric field (918 data points, green closed circles in Figure 1). Figure 2 shows some representative structures for all the four classes of HCl-(DMSO)$_n$ clusters. An alternative way to analyze the present set of results is depicted in Figure 1B. The two sets of data, the undissociated and the dissociated HCl-(DMSO)$_n$ clusters are fitted separately to straight lines, and the data points that lie in the range 133–171 MV cm^{-1} can be interpreted as bistable region, in which the HCl molecule could either dissociate or remain undissociated. The number of data points in the bistable region is 1220, of which 272 and 948 structures correspond to undissociated and dissociated structures, respectively. Further, it can be noticed that the data points corresponding to the dissociated form of HCl show a large scatter along the H–Cl distance axis, similar to the phenol-(ammonia)$_n$ clusters,[27] and unlike in the case of HCl dissociation in water clusters.[14] In the case of phenol-(ammonia)$_n$ clusters, the large scatter was attributed to the inability of the projection of the electric field along the OH bond distance as the proton-transfer-reaction coordinate involved out-of-plane motion of the OH group along with stretching of the OH bond.[27] However, in the case of HCl the dissociation involves a single bond stretching coordinate, therefore such scatter is unexpected. However, the bistability of the HCl dissociation indicates that the solvation environment of DMSO could play a pivotal role, unlike in the case of water.[14]

In order to raise the confidence level of the present work, 644 HCl-(DMSO)$_n$ structures were reoptimized at MP2/6-31+G(d,p), which also included 131 structures out of 189 data points corresponding to the exceptions (shown as red open circles in Figure 1), wherein the electric field is higher than the critical electric field, yet the HCl remains undissociated. Among these 131 data points, only two instances of undissociated structures at the B3LYP-D3 level resulted in dissociated structures at the MP2 level. Following MP2/6-31+G(d,p) re-optimization, the electric field along the H–Cl bond was calculated and the resulting plot of H–Cl bond distance against the corresponding electric field is shown in Figure 3, which shows a marked improvement over the corresponding plot shown in Figure 1A. The MP2/6-31+G(d,p) calculations yield 181 MV cm^{-1} as the critical electric field required for the dissociation of HCl in DMSO clusters. Interestingly, only 5 (five) exceptions with undissociated HCl with an electric field higher than the critical electric field of 181 MV cm^{-1} were observed. Error estimation based on

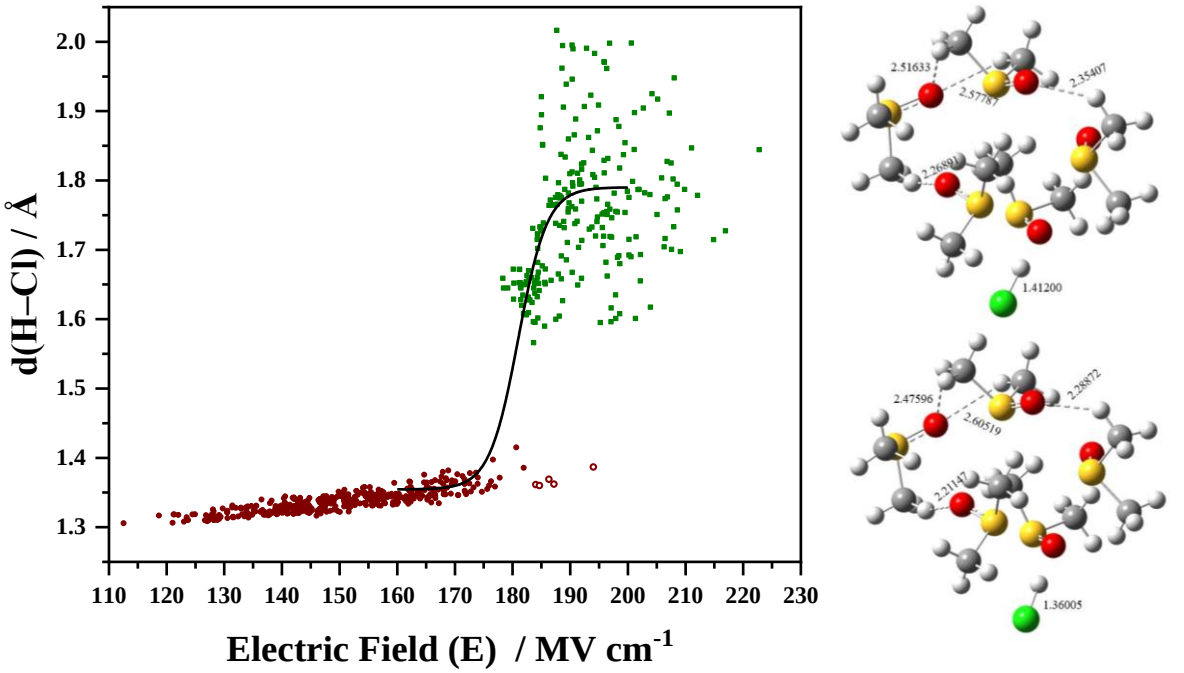

Figure 3. The plot of H–Cl distance against electric field calculated along the H–Cl bond in $HCl(DMSO)_n$ [n=2-5] clusters at MP2/6-31+G(d,p) level of theory. The data points in red circles and green squares correspond to the undissociated and dissociated HCl molecule, respectively. The solid curve is a non-linear Boltzmann sigmoidal fit to the data points with an R^2 value of 0.851 with the point of inflection at 181.0 MV cm^{-1}. The open red circles are exceptions to the sigmoidal fitting. The number of data points corresponding to undissociated and dissociated structures is 412 and 233, respectively. The right panel shows the representative structure of one of the $HCl(DMSO)_5$ cluster optimized by B3LYP-D3/6-311+G(d,p) (top) and MP2/6-31+G(d,p) (bottom) level, which suggest that the MP2 level yield compact cluster relative to the B3LYP-D3 level of calculation.

uncertainties in the H–Cl covalent bond and hydrogen bond distances of about 0.01 Å and 0.05 Å lead to uncertainty of 3-5 MV cm^{-1} in the electric fields. Therefore baring a single instance, there will be no exceptions in the case of MP2/6-31+G(d,p) calculations. The comparison of the electric fields along the H–Cl bond for the undissociated structures is in the range 103-171 and 112-194 MV cm^{-1} for the B3LYP-D3 and MP2 level calculations, with average values of 134.4 and 150.3 MV cm^{-1}, respectively. On the other hand, the electric fields for the dissociated structures are in the range 133-184 and 178-223 MV cm^{-1} for the B3LYP-D3 and MP2 level calculations, with average values of 149.3 and 192.2 MV cm^{-1}, respectively. The electric field data suggests that, in general, the B3LYP functional underestimate the electric field values relative to the MP2 calculations.

However, a comparison of the average values of the undissociated (134.4 vs. 150.3 MV cm^{-1}) and dissociated (149.3 vs.192.2 MV cm^{-1}) structures indicates that the electric field estimation by the B3LYP functional for the dissociated structures is unusually low.

The electric field is a local descriptor based on the cluster structure, A careful examination of the structure reveals that optimization by the MP2 method leads to a more compact structure in terms of intermolecular contacts, even though the gross shape of the cluster remains very similar, as depicted in a representative set of structures optimized at the B3LYP-D3 and MP2 methods in Figure 3. Further, the structural similarity analysis between the B3LYP-D3 and MP2 optimized structures was carried out using the ultrafast shape recognition (USR) technique.[20] For a given pair of geometries optimized by B3LYP-D3 and MP2 methods, we compare their spatial atomic distributions

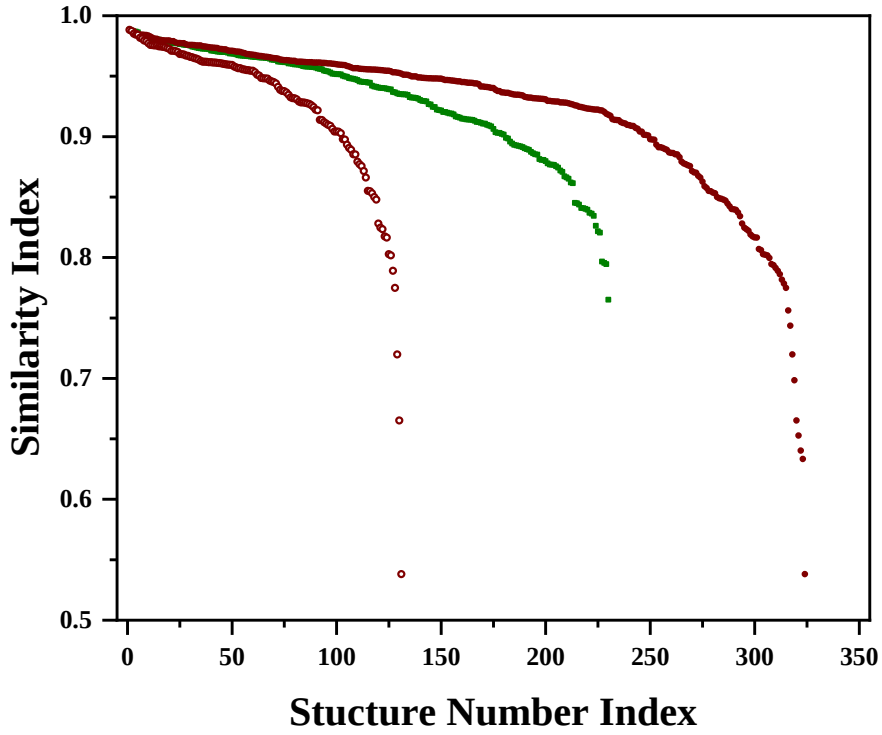

Figure 4. The plot of structural similarity index between B3LYP-D3/6-311+G(d) and MP2/6-31+G(d,p) optimized structures. In this plot, the green closed squares, red closed circles and red open circles correspond to structures in which HCl is dissociated, undissociated and exceptions at B3LYP-D3 level, respectively. Note that the exceptions (red open circles) are a subset of undissociated structures (red closed circles). The comparison suggests that out of 554 structures, only 22 structures have a similarity index less than 0.8, which indicates that in general the gross structure of the cluster remains almost unaltered.

and compute the normalized similarity index in a range from the least similar (0) to identical shape (1). The resulting similarity indexes are compiled in Figure 4. we had carried out MP2 re-optimization on 644 geometries of HCl-(DMSO)n obtained by B3LYP-D3, there are 230 dissociated and 324 undissociated structures found in both levels of theory. The comparison suggests that out of 554 (230+324) structures, only 22 structures have a similarity index less than 0.8, which indicates that in general the gross structure of the cluster remains almost unaltered. Among the remaining 90 structures (644 - 554), only 3 cases were observed wherein undissociated HCl at the B3LYP-D3 level is dissociated at MP2 level. On the other hand, a large fraction of dissociated structures (87 data points) at the B3LYP-D3 level remain undissociated at the MP2 level. This observation can be attributed to the lower proton transfer barrier for the B3LYP functional.[31] Further, it can be noted that in general, the electric field values calculated using the B3LYP functional are lower than the corresponding MP2 values, especially for the dissociated structures. To probe the role of B3LYP functional on the electric field values, a set of twenty (20) dissociated structures with both B3LYP-D3 and MP2 geometries available were chosen. For these set of structures, the and the electric fields along the H–Cl bond were calculated as (i) B3LYP field at B3LYP-D3 geometry, (ii) B3LYP field at MP2 geometry, (iii) MP2 field at MP2 geometry, (iv) MP2 field at B3LYP-D3 geometry and (v) RHF field at B3LYP-D3 geometry and the results are presented in Figure 5A. The calculations reveal that in general the B3LYP functional underestimates the electric field values for the dissociated structures by about 40 MV cm^{-1}. Surprisingly, even the RHF calculations estimate the electric fields which are comparable with the MP2 calculations, which indicates the importance of HF exchange.[31] The electric field data obtained from the B3LYP functional were increased by 15.9 and 42.9 MV cm^{-1} for the undissociated and dissociated structures, respectively, which corresponds to the difference in the average values obtained by the B3LYP functional and MP2 method, *vide supra*. The resulting plot is shown in Figure 5B, and the data points could be fitted to Boltzmann sigmoidal function with the critical electric field value of 176.9 MV cm^{-1}, without only five (5) exceptions, similar to MP2 calculations (see Figure 3A and the associated text). Invoking uncertainties of 3-5 MV cm^{-1} in the electric field calculations, *vide supra*, only one data point would be an exception, once again in agreement with the MP2 method. Moreover, the critical electric fields required for the HCl dissociation are 176.9 and 181.0 MV cm^{-1} using B3LYP functional and MP2 method are comparable. It is

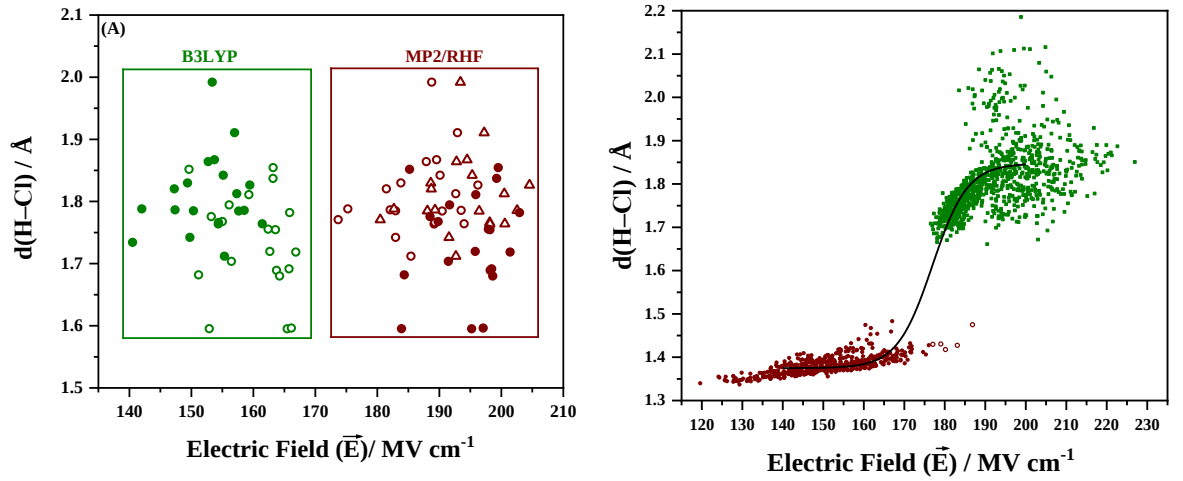

Figure 5. (A) The plot of H–Cl distance against electric field calculated along the H–Cl bond in selected dissociated HCl(DMSO)$_n$ clusters. The solid and open green circles correspond to electric fields calculated using B3LYP functional for B3LYP-D3 and MP2 geometries, respectively. On the other hand, the solid and open red circles correspond to electric fields calculated using the MP2 method for MP2 and B3LYP-D3 geometries, respectively. The red open triangles depict electric field values calculated using the RHF method using B3LYP-D3 geometries. (B) The plot of H–Cl distance against electric field calculated along the H–Cl bond in HCl(DMSO)$_n$ [n=2-5] clusters at B3LYP-D3/6-311+G(d,p) level of theory. The data points in red circles and green squares correspond to the undissociated and dissociated HCl molecule, respectively. In this case, the electric fields for the undissociated and dissociated HCl molecule were increased by 15.9 and 42.9 MV cm^{-1}, respectively, which corresponds to the difference in the average values obtained by B3LYP functional and MP2 methods. The solid curve is a non-linear Boltzmann sigmoidal fit to the data points, excluding the red open circles, with an R^2 value of 0.929 with the point of inflection at 176.9 MV cm^{-1}

well-known in the literature that B3LYP functional is unable to model the dispersion non-covalent interactions especially the dispersion interactions very accurately.[32] A significant improvement in the ability of the B3LYP functional to model the non-covalent interactions by using pair-wise dispersion parameters,[33] which modifies the B3LYP energy and not the underlying electronic structure predicted by the method itself. The present work on the dissociation of HCl embedded in DMSO clusters and the concurrent proton transfer reaction using B3LYP functional indicates that the critical electric field is necessary, but it is not a sufficient condition for HCl dissociation.[27] On the other hand, the MP2 calculations signify that critical electric field indeed a both necessary and a sufficient condition. The calculations using B3LYP functional grossly underestimate the MESP values consequently the electric field values for the proton transferred structures, which

can be related to the quality of the associated wavefunction. Therefore, electric field calculations are a very helpful tool to quickly test the efficiency of the level of theory used to model the interactions present in the system of interest, especially in the case of proton transfer reactions. More importantly, to understand the proton transfer reactions B3LYP functional must be used with caution and the observed bistability of HCl dissociation in DMSO appears to be an artefact.

CONCLUSIONS

In this study dissociation of HCl embedded in DMSO, clusters was investigated with the aid of internal electric fields as a descriptor for the dissociation process, using B3LYP-D3/6-311+g(d,p) and MP2/6-31+g(d,p) levels of theory. A large data set was employed in this regard so that that the results are statistically reliable. The B3LYP calculations suggest that a critical electric field of about 137 MV cm^{-1} along the H–Cl bond was required for it to dissociate in DMSO clusters. However, a large number of exceptions to the phenomena of critical electric field promoting the acid dissociation were observed, wherein in several clusters with the electric field values much higher than 137 MV cm^{-1} did not result in dissociation in addition to some clusters which resulted in the dissociation with the field less than the critical electric field. On the other hand, the MP2 level calculations reveal that a critical electric field of 181 MV cm^{-1} along the H–Cl bond was required for it to dissociate, with almost no exceptions. The present work reveals that the calculations using B3LYP functional lead to an artefact in the plot of H–Cl distance vs. electric field which indicates its inability of this functional to model proton transfer process adequately and care must be exercised in interpreting processes involving such phenomena.

ACKNOWLEDGEMENTS

D.S. thanks IITB-Monash Research Academy for the fellowship. DS and GNP gratefully acknowledge the SpaceTime-2 supercomputing facility at IIT Bombay for the computing time. PJH and JLK were supported by Academia Sinica and the Ministry of Science and Technology of Taiwan (MOST107-2628-M-001-002-MY4, MOST109-2639-M-009-001-

ASP, and MOST109-2113-M-001-040). PJH would like to thank Academia Sinica Postdoctoral Research Fellowship to support the initial stage of this work.

The authors declare no competing interest.

REFERENCES

1 A. Trummal, L. Lipping, I. Kaljurand, I. A. Koppel and I. Leito, Acidity of Strong Acids in Water and Dimethyl Sulfoxide, *J. Phys. Chem. A*, 2016, **120**, 3663–3669.

2 A. Kütt, T. Rodima, J. Saame, E. Raamat, V. Mäemets, I. Kaljurand, I. A. Koppel, R. Y. Garlyauskayte, Y. L. Yagupolskii, L. M. Yagupolskii, E. Bernhardt, H. Willner and I. Leito, Equilibrium acidities of superacids, *J. Org. Chem.*, 2011, **76**, 391–395.

3 F. G. Bordwell, Equilibrium Acidities in Dimethyl Sulfoxide Solution, *Acc. Chem. Res.*, 1988, **21**, 456–463.

4 K. R. Srivastava, B. Goyal, A. Kumar and S. Durani, Scrutiny of electrostatic-driven conformational ordering of polypeptide chains in DMSO: A study with a model oligopeptide, *RSC Adv.*, 2017, **7**, 27981–27991.

5 K. Raj Srivastava, A. Kumar, B. Goyal and S. Durani, Stereochemistry and solvent role in protein folding: Nuclear magnetic resonance and molecular dynamics studies of poly-L and alternating-L,D homopolypeptides in dimethyl sulfoxide, *J. Phys. Chem. B*, 2011, **115**, 6700–6708.

6 A. M. S. Duarte, C. P. M. Van Mierlo and M. A. Hemminga, Molecular dynamics study of the solvation of an α-helical transmembrane peptide by DMSO, *J. Phys. Chem. B*, 2008, **112**, 8664–8671.

7 W. Dzwolak, J. Kalinowski, C. Johannessen, V. Babenko, G. Zhang and T. A. Keiderling, On the DMSO-dissolved state of insulin: A vibrational spectroscopic study of structural disorder, *J. Phys. Chem. B*, 2012, **116**, 11863–11871.

8 U. T. Sankpal, M. Abdelrahim, S. F. Connelly, C. M. Lee, R. Madero-Visbal, J. Colon, J. Smith, S. Safe, P. Maliakal and R. Basha, Small molecule tolfenamic acid inhibits PC-3 cell proliferation and invasion in vitro, and tumor growth in orthotopic mouse model for prostate cancer, *Prostate*, 2012, **72**, 1648–1658.

9 C. T. Wohnhaas, G. G. Leparc, F. Fernandez-Albert, D. Kind, F. Gantner, C. Viollet, T. Hildebrandt and P. Baum, DMSO cryopreservation is the method of choice to preserve cells for droplet-based single-cell RNA sequencing, *Sci. Rep.*, 2019, **9**, 1–14.

10 K. I. Oh, K. Rajesh, J. F. Stanton and C. R. Baiz, Quantifying Hydrogen-Bond Populations in Dimethyl Sulfoxide/Water Mixtures, *Angew. Chemie - Int. Ed.*, 2017, **56**, 11375–11379.

11 A. Idrissi, B. A. Marekha, M. Barj, F. A. Miannay, T. Takamuku, V. Raptis, J. Samios and P. Jedlovszky, Local structure of dilute aqueous DMSO solutions, as seen from molecular dynamics simulations, *J. Chem. Phys.*, 2017, **146**, 234507.

12 K. I. Oh, X. You, J. C. Flanagan and C. R. Baiz, Liquid-Liquid Phase Separation Produces Fast H-Bond Dynamics in DMSO-Water Mixtures, *J. Phys. Chem. Lett.*, 2020, **11**, 1903–1908.

13 J. Catalán, C. Díaz and F. García-Blanco, Characterization of binary solvent mixtures of DMSO with water and other cosolvents, *J. Org. Chem.*, 2001, **66**, 5846–5852.

14 M. Boda and G. Naresh Patwari, Insights into acid dissociation of HCl and HBr with internal electric fields, *Phys. Chem. Chem. Phys.*, 2017, **19**, 7461–7464.

15 Q. Cui, M. Elstner, E. Kaxiras, T. Frauenheim and M. Karplus, A QM/MM implementation of the self-consistent charge density functional tight binding (SCC-DFTB) method, *J. Phys. Chem. B*, 2001, **105**, 569–585.

16 H. A. Witek and K. Morokuma, Systematic study of vibrational frequencies calculated with the self-consistent charge density functional tight-binding method, *J. Comput. Chem.*, 2004, **25**, 1858–1864.

17 H. Yu and Q. Cui, The vibrational spectra of protonated water clusters: A benchmark for self-consistent-charge density-functional tight binding, *J. Chem. Phys.*, 2007, **127**, 234504.

18 M. Gaus, Q. Cui and M. Elstner, DFTB3: Extension of the self-consistent-charge density-functional tight-binding method (SCC-DFTB), *J. Chem. Theory Comput.*, 2011, **7**, 931–948.

19 T. D. Kühne, M. Iannuzzi, M. Del Ben, V. V. Rybkin, P. Seewald, F. Stein, T. Laino, R. Z. Khaliullin, O. Schütt, F. Schiffmann, D. Golze, J. Wilhelm, S. Chulkov, M. H. Bani-Hashemian, V. Weber, U. Borštnik, M. Taillefumier, A. S. Jakobovits, A. Lazzaro, H. Pabst, T. Müller, R. Schade, M. Guidon, S. Andermatt, N. Holmberg, G. K. Schenter, A. Hehn, A. Bussy, F. Belleflamme, G. Tabacchi, A. Glöß, M. Lass, I. Bethune, C. J. Mundy, C. Plessl, M. Watkins, J. VandeVondele, M. Krack and J. Hutter, CP2K: An electronic structure and molecular dynamics software package -Quickstep: Efficient and accurate electronic structure calculations, *J. Chem. Phys.*, 2020, **152**, 194103.

20 P. J. Ballester, P. W. Finn and W. G. Richards, Ultrafast shape recognition: Evaluating a new ligand-based virtual screening technology, *J. Mol. Graph. Model.*, 2009, **27**, 836–845.

21 H. Kruse, L. Goerigk and S. Grimme, Why the standard B3LYP/6-31G* model chemistry should not be used in DFT calculations of molecular thermochemistry: Understanding and correcting the problem, *J. Org. Chem.*, 2012, **77**, 10824–10834.

22 M. J. Frisch, G. W. Trucks, H. B. Schlegel, G. E. Scuseria, M. A. Robb, J. R. Cheeseman, G. Scalmani, V. Barone, G. A. Petersson, H. Nakatsuji, X. Li, M. Caricato, A. V. Marenich, J. Bloino, B. G. Janesko, R. Gomperts, B. Mennucci, H. P. Hratchian, J. V. Ortiz, A. F. Izmaylov, J. L. Sonnenberg, D. Williams-Young, F. Ding, F. Lipparini, F. Egidi, J. Goings, B. Peng, A. Petrone, T. Henderson, D. Ranasinghe, V. G. Zakrzewski, J. Gao, N. Rega, G. Zheng, W. Liang, M. Hada, M. Ehara, K. Toyota, R. Fukuda, J. Hasegawa, M. Ishida, T. Nakajima, Y. Honda, O. Kitao, H. Nakai, T. Vreven, K. Throssell, J. Montgomery, J. A., J. E. Peralta, F. Ogliaro, M. J. Bearpark, J. J. Heyd, E. N. Brothers, K. N. Kudin, V. N. Staroverov, T. A. Keith, R. Kobayashi, J. Normand, K. Raghavachari, A. P. Rendell, J. C. Burant, S. S. Iyengar, J. Tomasi, M. Cossi, J. M. Millam, M. Klene, C. Adamo, R. Cammi, J. W. Ochterski, R. L. Martin, K. Morokuma, O. Farkas, J. B. Foresman and D. J. Fox, *Gaussian 16, Revision B.01*, Gaussian, Inc.,

Wallingford, CT,2016.

23 P. Hsu, K. Ho, S. Lin and J. Kuo, Exploration of hydrogen bond networks and using a two-stage clustering algorithm †, *Phys.Chem.Chem.Phys.*, 2017, **19**, 544–556.

24 A. Fujii, N. Sugawara, P. J. Hsu, T. Shimamori, Y. C. Li, T. Hamashima and J. L. Kuo, Hydrogen bond network structures of protonated short-chain alcohol clusters, *Phys. Chem. Chem. Phys.*, 2018, **20**, 14971–14991.

25 S. Mishra, D. K. Sahoo, P. J. Hsu, Y. Matsuda, J. L. Kuo, H. S. Biswal and G. N. Patwari, A liquid crucible model for aggregation of phenylacetylene in the gas phase, *Phys. Chem. Chem. Phys.*, 2019, **21**, 13623–13632.

26 S. Singh, P.-J. Hsu, J.-L. Kuo and G. N. Patwari, Dipole moment enhanced π–π stacking in fluorophenylacetylenes is carried over from gas-phase dimers to crystal structures propagated through liquid like clusters, *Phys. Chem. Chem. Phys.*, 2021, **23**, 9938–9947.

27 D. Sadhukhan, A. Hazra and G. Naresh Patwari, Bend-to-Break: Curvilinear Proton Transfer in Phenol-Ammonia Clusters, *J Phys Chem A*, 2020, **124**, 3101–3108.

28 S. Sen, M. Boda, S. Venkat Lata and G. Naresh Patwari, Internal electric fields in small water clusters [$(H_2O)_n$; n = 2–6], *Phys. Chem. Chem. Phys.*, 2016, **18**, 16730–16737.

29 M. Saggu, N. M. Levinson and S. G. Boxer, Experimental quantification of electrostatics in X-H···φ hydrogen bonds, *J. Am. Chem. Soc.*, 2012, **134**, 18986–18997.

30 M. Saggu, N. M. Levinson and S. G. Boxer, Direct measurements of electric fields in weak OH···π hydrogen bonds, *J. Am. Chem. Soc.*, 2011, **133**, 17414–17419.

31 G. F. Mangiatordi, E. Brémond and C. Adamo, DFT and proton transfer reactions: A benchmark study on structure and kinetics, *J. Chem. Theory Comput.*, 2012, **8**, 3082–3088.

32 G. A. DiLabio, M. Koleini and E. Torres, Extension of the B3LYP-dispersion-correcting potential approach to the accurate treatment of both inter-and intra-molecular interactions, *Theor. Chem. Acc.*, 2013, **132**, 1–13.

33 S. Grimme, J. Antony, S. Ehrlich and H. Krieg, A consistent and accurate ab initio parametrization of density functional dispersion correction (DFT-D) for the 94 elements H-Pu, *J. Chem. Phys.*, 2010, **132**, 154104.